

**Muon beam experiments to probe the dark sector**Chien-Yi Chen,<sup>1,2,\*</sup> Maxim Pospelov,<sup>1,2,†</sup> and Yi-Ming Zhong<sup>3,‡</sup><sup>1</sup>*Department of Physics and Astronomy, University of Victoria,  
Victoria, British Columbia V8P 5C2, Canada*<sup>2</sup>*Perimeter Institute for Theoretical Physics, Waterloo, Ontario N2J 2W9, Canada*<sup>3</sup>*Physics Department, Boston University, Boston, Massachusetts 02215, USA*

(Received 24 February 2017; published 6 June 2017)

A persistence of several anomalies in muon physics, such as the muon anomalous magnetic moment and the muonic hydrogen Lamb shift, hints at new light particles beyond the Standard Model. We address a subset of these models that have a new light scalar state with sizable couplings to muons and suppressed couplings to electrons. A novel way to search for such particles would be through muon beam-dump experiments by (1) missing momentum searches; (2) searches for decays with displaced vertices. The muon beams available at CERN and Fermilab present attractive opportunities for exploring the new scalar with a mass below the dimuon threshold, and potentially covering a range of relevant candidate models. For the models considered in this paper, both types of signals, muon missing momentum and anomalous energy deposition at a distance, can probe a substantial fraction of the unexplored parameter space of the new light scalar, including a region that can explain the muon anomalous magnetic moment discrepancy.

DOI: 10.1103/PhysRevD.95.115005

**I. INTRODUCTION**

New physics (NP) at low-mass, treated in all generality, has become an actively pursued topic of the intensity frontier physics [1–3] given the abundant evidence for NP in the neutrino and dark matter sectors, coupled with the lack of NP signal at the Large Hadron Collider (LHC). Motivations for searches of low-mass, weakly-coupled particles can come from top-down theoretical arguments (see *e.g.* [4]). But a bigger role is played by the existing anomalous observations in particle experiments, astrophysics, and cosmology, which might find their explanations in models with NP at low-mass (see *e.g.* [5–7]). The current  $\sim 3.5\sigma$  discrepancy between the predicted and observed value of the muon anomalous magnetic moment [8],  $a_\mu$ , will be scrutinized in the upcoming experiments at Fermilab and JPARC [9,10]. It is not clear that the current tension is a result of experimental errors or theoretical errors or a combination of the two. With new measurements of muon  $g-2$  and improved Standard Model (SM) calculations based on lattice QCD [11,12], one hopes to clarify the origin of the existing discrepancy. Lamb shifts of muonic atoms, such as muonic hydrogen and deuterium [13–15], present another formidable puzzle. When interpreted in terms of the charge radius of the proton,  $r_p$ , these measurements disagree with the electron scattering and hydrogen spectroscopy extracted values of  $r_p$  by  $\sim 7\sigma$  [16].

In this paper, we are interested in the scenarios where the deficit of theoretical predictions for  $a_\mu$  is compensated by a

contribution from NP. Although the overall size of the  $a_\mu$  discrepancy,  $a_\mu^{\text{obs}} - a_\mu^{\text{th}} \approx +3 \times 10^{-9}$ , is on the order of the corresponding contributions from the weak sector of the SM, the NP states correcting the anomalous magnetic moment do not have to reside at the weak scale. Indeed it is well known that the existing theoretical deficit can be compensated by loop contributions from new light particles [17–19]. One such candidate model, the dark photon, has been searched for in a variety of experiments, with recent results ruling out the most minimal version as a possible explanation of the  $a_\mu$  discrepancy. Some other candidate models still survive the existing constraints, including the  $L_\mu - L_\tau$  gauged model and its variations [20,21].

Here we would like to examine the models with a new light scalar,  $S$ , tuned to explain the  $a_\mu$  discrepancy [22,23]. We will employ a simplified framework, with a relevant Lagrangian given by

$$\mathcal{L} \supset \frac{1}{2}(\partial_\mu S)^2 - \frac{1}{2}m_S^2 S^2 - \sum_{\ell=e,\mu,\tau} g_\ell S \bar{\ell} \ell, \quad (1)$$

where  $g_\ell$  is the coupling between  $S$  and leptons. Notice that Eq. (1) is an effective Lagrangian that does not respect the full gauge symmetry of the SM. Its  $SU(2) \times U(1)$  generalization is given by the following dimension-five effective operator,

$$\mathcal{O}_5 = \frac{1}{\Lambda} (\bar{L}E)HS, \quad (2)$$

where  $H$  is the SM Higgs doublet, and  $L$ ,  $E$  are the lepton doublets and singlets respectively. The effective operator,  $\mathcal{O}_5$ , can be embedded into a full model in a variety of ways.

\*cchen@perimeterinstitute.ca

†mpospelov@perimeterinstitute.ca

‡ymzhong@bu.edu

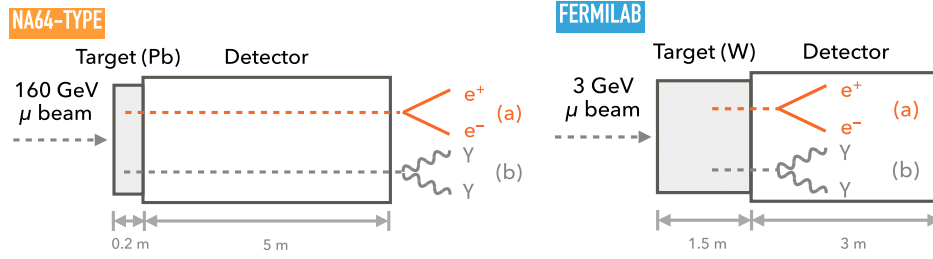


FIG. 1. Setups for muon beam-dump experiments at NA64 (left) and Fermilab (right). For the NA64-type experiment, the muon beam energy is  $\sim 160$  GeV and the target material is lead. We focus on the missing energy searches with  $S$  decays into  $e^+e^-$  (a) and  $\gamma\gamma$  (b). For Fermilab experiment, the muon beam energy is  $\sim 3$  GeV and the target material is tungsten. We focus on the decays with displaced vertices of  $S$ . The lengths of the targets and the detectors are shown in the plot.

References [22,23] discuss the phenomenology of such a model and choose different types of UV completion of  $\mathcal{O}_5$  with vector-like fermions or multiple Higgs states respectively. The latter UV completion generates strong constraints for the mass range  $m_S > 2m_\mu$  due to recent searches of unexpected peaks in the dimuon mass spectrum for  $B \rightarrow K(\mu^+\mu^-)$  decays at the LHCb [24]. The mass range of  $m_S < 2m_\mu$  remains largely unexplored. In this mass range, the new light particles can be relatively long-lived, and thus amenable to beam-dump experiments and fixed-target searches.

In this paper, we investigate the potential of experiments where the light scalar,  $S$ , is sourced by the collision of muons with nuclei. Subsequent displaced decays of  $S$  present an opportunity for both the missing momentum and the anomalous energy deposition searches. We take the existing CERN and Fermilab muon<sup>1</sup> sources as an example and illustrated our main idea in Fig. 1. For a NA64-type setup at CERN [25,26], the *dark* emission of  $S$  states with  $S$  decaying outside of the detector would cause the anomalous loss of muon energy, which can be detected in the muon scattering experiment. The muon beam with beam energy around a few GeV at Fermilab would also provide a great opportunity. Here muons are stopped in the dense material, and subsequent anomalous energy deposition is searched directly behind it. In what follows, we demonstrate that both approaches allow probing unexplored parts of the parameter space of the simplified model potentially responsible for the  $a_\mu$  discrepancy. We use the bremsstrahlung,  $\mu^+ + N \rightarrow \mu^+ + N + S$ , as the main production mechanism as illustrated in Fig. 2, where an incident muon,  $\mu^+$ , interacts with a target nucleus,  $N$ , by exchanging a photon,  $\gamma$ , and radiates the exotic scalar,  $S$ . The two muon beam-dump experiments considered in this paper can be easily implemented with only modest modifications/additions to the existing experimental infrastructure. Looking into more distant future, the proton beam-dump facilities,

<sup>1</sup>“Muon” or “ $\mu$ ” refers to  $\mu^+$  for the muon beam-dump experiments.

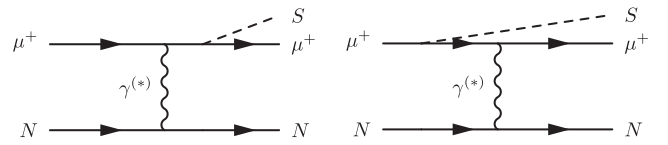


FIG. 2. Feynman diagrams illustrating the bremsstrahlung production of the new light states,  $S$ , where an incoming muon,  $\mu^+$ , interacts with a target nucleus,  $N$ , by exchanging a photon,  $\gamma$ , and radiates the exotic scalar,  $S$ .

such as SHiP [27], would also provide strong sensitivities to muon-coupled light states.

The paper is organized as follows: We first show two specifications of the simplified model in Sec. II and analyze the two proposed muon beam-dump experiments in Sec. III. We show the resulting expected sensitivities in Sec. IV, conclude, and discuss other related experiments in Sec. V.

## II. MODELS WITH NEW LIGHT SCALARS

For the simplified model introduced in the previous section, Eq. (1), the couplings  $g_{\ell=e,\mu,\tau}$  are free parameters. The muon anomalous magnetic moment,  $a_\mu$ , receives corrections due to the one-loop contribution of  $S$ ,

$$\Delta a_\mu = \frac{g_\mu^2}{8\pi^2} \int_0^1 dz \frac{(1-z)^2(1+z)}{(1-z)^2 + z(m_S/m_\mu)^2}. \quad (3)$$

Requiring this correction to reduce current tension between measurement and the SM calculation of  $a_\mu$ , one arrives at the preferred values of  $\{g_\mu, m_S\}$  parameters. For example, given  $g_\mu = 5 \times 10^{-4}$  and  $m_S = 100$  MeV,  $\Delta a_\mu$  is around  $1.6 \times 10^{-9}$ . This would bring the theoretical and experimental values for the muon anomalous magnetic moment within  $2\sigma$ . Other couplings,  $g_e$  and  $g_\tau$ , still remains free. Here we will consider two models with further specifications on the couplings of  $g_e$  and  $g_\tau$ :

- (i) Model A: Mass proportionality,  $g_\ell \propto m_\ell$ . In particular, it implies that the couplings between the scalar  $S$  and electrons are  $\sim 200$  times smaller than those with

muons. Despite this, the dominant decay channel for  $S$  below the dimuon threshold is  $S \rightarrow e^+e^-$ .

- (ii) Model B: Coupling exclusively to muons,  $g_\mu \neq 0$  and  $g_e = g_\tau = 0$ . This is the most collider and electron/proton beam-dumps unfriendly case, that still can be relevant for the muon  $g-2$ . Due to the longer lifetime of  $S$ , the missing energy search at NA64-type experiments would be particularly useful to constrain the parameter space of this model.

Model A can be explicitly constructed using the leptonic Higgs doublet model completion of Ref. [23]. In that model, the lepton flavor conservation and  $g_\ell \propto m_\ell$  proportionality are guaranteed, as only one Yukawa matrix determines the lepton masses and their couplings to  $S$ . Model B is in some sense more artificial but phenomenologically minimal. Only one coupling is introduced that is necessary to correct  $a_\mu$  in this model.

In both models,  $S$  dominantly decays to  $\mu^+\mu^-$  for  $2m_\mu < m_S < 2m_\tau$ . For the mass range that we concentrate on,  $2m_e < m_S < 2m_\mu$ , the total decay width,  $\Gamma_S$ , is a sum of the decay widths of  $S \rightarrow e^+e^-$  and  $S \rightarrow \gamma\gamma$  channels. They are respectively given by

$$\Gamma_{e^+e^-} = \frac{m_S}{8\pi} g_e^2 \left(1 - \frac{4m_e^2}{m_S^2}\right)^{3/2} \quad (4)$$

and

$$\Gamma_{\gamma\gamma} = \frac{\alpha^2 m_S^3}{64\pi^3} \sum_{\ell=e,\mu,\tau} \frac{g_\ell^2}{m_\ell^2} |\tau_\ell [1 + (1 - \tau_\ell)f(\tau_\ell)]|^2, \quad (5)$$

where  $\tau_\ell \equiv 4m_\ell^2/m_S^2$  and the loop function  $f(\tau)$  reads,

$$f(\tau) = \begin{cases} \arcsin^2(\tau^{-1/2}), & \tau > 1 \\ -\frac{1}{4} \left[ \ln\left(\frac{1+\sqrt{1-\tau}}{1-\sqrt{1-\tau}}\right) - i\pi \right]^2, & \tau \leq 1 \end{cases} \quad (6)$$

For model A, the decay is dominantly through  $S \rightarrow e^+e^-$ ,

$$\Gamma_S^A = \Gamma_{e^+e^-} + \Gamma_{\gamma\gamma} \approx \Gamma_{e^+e^-} \quad (7)$$

For model B, the only decay channel is  $S \rightarrow \gamma\gamma$  via  $\mu$  loop, i.e.,

$$\Gamma_S^B = \frac{\alpha^2 m_S^3}{64\pi^3} \frac{g_\mu^2}{m_\mu^2} |\tau_\mu [1 + (1 - \tau_\mu)f(\tau_\mu)]|^2 \quad (8)$$

Given  $\Gamma_S$ , the decay length of the scalar  $S$  is expressed by

$$L_S = \frac{E_S \beta_S}{m_S \Gamma_S}, \quad (9)$$

where  $E_S$  is the energy of the scalar and the boost factor  $\beta_S = \sqrt{1 - m_S^2/E_S^2}$ . In particular, taking a fiducial choice

of parameters, and the energy of the scalar  $E_S = 3$  GeV, we find

$$L_S = 25 \text{ cm} \times \left(\frac{5 \times 10^{-4}}{g_\mu}\right)^2 \times \left(\frac{100 \text{ MeV}}{m_S}\right)^2, \quad \text{Model A,} \quad (10)$$

$$L_S = 20 \text{ m} \times \left(\frac{5 \times 10^{-4}}{g_\mu}\right)^2 \times \left(\frac{100 \text{ MeV}}{m_S}\right)^4, \quad \text{Model B.} \quad (11)$$

These sizable decay lengths give a good motivation to search for  $S$  in the beam-dump experiments.

A previous study of the muon-beam-initiated emission of axionlike particles, [28], shares several common features with our scalar model. Light dark vector particles emitted from a muon beam, in the context of the NA64 experiment, have been also studied in [26]. Our paper aims to extend these previous works to the scalar case, and explore the sensitivity reach on the  $m_S$ - $g_\mu$  parameter space.

### III. SIGNALS AND BACKGROUNDS

#### A. Signals

##### 1. NA64-type muon beam-dump experiment

In this subsection we investigate the constraints from the NA64-type experiment at CERN. NA64 is a fixed-target experiment searching for dark sector particles and kaon invisible decays at the CERN Super Proton Synchrotron (SPS). The detailed setup of the NA64 experiment can be found in Refs. [25,26], and the experiment has reported its first results from the  $2.75 \times 10^9$  electrons on target in 2017 [29]. We adopt similar geometries of the target and detector as suggested in Refs. [25,26] and sketch the setup in Fig. 1. The target is made of lead (Pb) with a thickness of  $\sim 20$  cm. The length of the detector is  $\sim 5$  meters. As pointed out in Ref. [26], the muon beam has a maximum luminosity of  $10^6$  muons per second in order to evade loss of the signal efficiency due to the pileup effect. We assume a three-month run of the experiment at the maximum luminosity, which yields  $8 \times 10^{12}$  muons in total on target. The incident muon beam energy,  $E_{\mu,\text{beam}}$ , is assumed to be around 160 GeV.

To estimate the reach, we need to calculation of the differential cross section of the beam-dump process  $\mu^+ + N \rightarrow \mu^+ + N + S$  as shown in Fig. 2. Given the large muon beam energy of NA64, we use the improved Weizsacker-Williams (IWW) approximation [30] in the evaluation.

When the beam energy is far greater than the mass of beam particle and the mass of produced particle,  $E_{\text{beam}} \gg m_{\text{beam}}, m_S$ , virtual photons generated by the highly-boosted beam particle are nearly transverse and behave as plane waves. Then the virtual photon can be

approximate as a real photon, and the phase space integration of a  $2 \rightarrow 3$  ( $\mu^+ + N \rightarrow \mu^+ + N + S$ ) process is simplified to a  $2 \rightarrow 2$  ( $\mu^+ + \gamma \rightarrow \mu^+ + S$ ) process. This is the so-called Weizsacker-Williams (WW) approximation [30]. The WW approximation can be further refined by using the fact that the production of  $S$  is dominantly collinear when the energy of  $S$  approaches the energy of  $\mu$ . This yields the improved Weizsacker-Williams (IWW) approximation where the integration limits on the virtuality,  $t$ , are further simplified [30,31]. The original IWW derivation [30,31] regards the beam particle to be massless. A detailed derivation of IWW with massive beam particles is presented in [32]. The resulting differential cross section is given by

$$\frac{d}{dx} \sigma(\mu^+ + N \rightarrow \mu^+ + N + S) \approx \frac{g_\mu^2 \alpha^2}{4\pi} \chi \beta_\mu \beta_S \frac{x^3 [m_\mu^2 (3x^2 - 4x + 4) + 2m_S^2 (1-x)]}{[m_S^2 (1-x) + m_\mu^2 x^2]^2}, \quad (12)$$

where  $x \equiv E_S/E_\mu$  is the ratio between the energy of the exotic scalar,  $E_S$ , and the energy of the muon,  $E_\mu$ , inside the material. The boost factor for muon and the new scalar are given respectively by  $\beta_\mu = \sqrt{1 - m_\mu^2/E_\mu^2} \approx 1$  and  $\beta_S = \sqrt{1 - m_S^2/(xE_\mu)^2}$ . The effective photon flux,  $\chi$ , is given by

$$\chi = \int_{t_{\min}}^{t_{\max}} dt \frac{t - t_{\min}}{t^2} G_2(t) \approx \int_{m_S^2/(4E_\mu^2)}^{m_S^2 + m_\mu^2} dt \frac{t - m_S^2/(4E_\mu^2)}{t^2} G_2(t), \quad (13)$$

where  $G_2$  is the combined atomic and nuclear form factor. The explicit expression of  $G_2$  is given in the appendix. The simplified integration on  $t$  from the IWW approximation is implemented in the second approximation of Eq. (13).

Unlike earlier studies for the dark sector searches via electron beam-dumps, here we keep the beam particle mass to be non-zero. As a consequence, the expected energy spectrum of  $S$  varies quite significantly as  $m_S$  increases. In Fig. 3, we demonstrate this point by comparing  $x$  spectrum for  $m_S = 10$  MeV and  $m_S = 100$  MeV. The emission of light particles ( $m_S \ll m_\mu$ ) clearly favors the low  $x$  region, while for  $m_S \approx m_\mu$ , the outgoing  $S$  takes more significant portion of the muon energy.

The total number of events,  $N_S$ , can be obtained as a convolution of the production cross section and the decay probability. It is given by

$$N_S = N_\mu \int_{y_{\min}}^{y_{\max}} dy n_{\text{atom}} \int_{x_{\min}}^1 dx \frac{d\sigma_{2 \rightarrow 3}}{dx} \int_{z_{\min}}^{z_{\max}} dz P(z) \quad (14)$$

$$= N_\mu \int_{y_{\min}}^{y_{\max}} dy n_{\text{atom}} \int_{x_{\min}}^1 dx \frac{d\sigma_{2 \rightarrow 3}}{dx} (e^{-\frac{z_{\min}}{L_S}} - e^{-\frac{z_{\max}}{L_S}}), \quad (15)$$

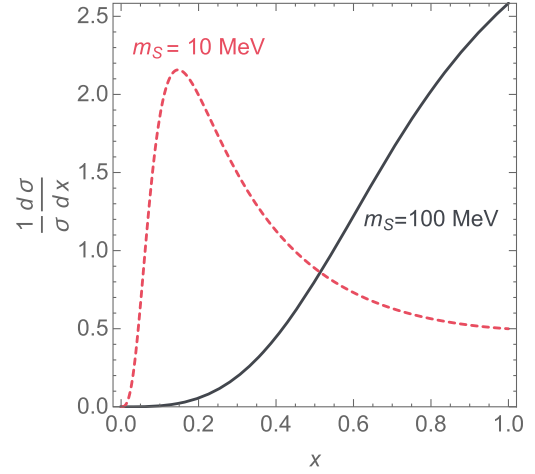


FIG. 3. Distributions of the fraction of the energy of the incident muon taken by the emission of an exotic scalar  $S$  for various scalar masses. The red dashed curve is for  $m_S = 10$  MeV and the black solid curve is for  $m_S = 100$  MeV.

where  $N_\mu$  is the total number of incident muons and  $\sigma_{2 \rightarrow 3}$  is a shorthand for  $\sigma(\mu^+ + N \rightarrow \mu^+ + N + S)$ .  $n_{\text{atom}}$  is the number density of target nuclei and its integration over the muon penetration length,  $y$ , accounts for the number of target nuclei that a incident muon encounters.  $P(z)$  stands for the decay probability density (per length) of  $S$  decaying within the fiducial decay range from  $z_{\min}$  to  $z_{\max}$ .  $L_S$  is the decay length given by Eq. (9) with  $E_S = E_\mu x$ . We also impose a  $x_{\min}$  in the integration over  $x$  to satisfy the specific requirements for the search of the signal.

Muon beams penetrate the target to a much longer depth compared to that of the electron beams. It can lose energy through multiple mechanisms [33]. For the energy range we are interested in, from a few GeV to  $\sim 100$  GeV, the muon energy loss is dominantly through the ionization and the stopping power  $\langle dE_\mu/dy \rangle$  is relatively flat with respect to the muon momentum [33]. Hence we approximate the muon energy loss per unit length  $\langle dE_\mu/dy \rangle$  to be a *constant*. Consequently  $E_\mu$  is related to the penetration length  $y$  via

$$\Delta y \equiv y - y_{\min} = \frac{E_{\mu, \text{beam}} - E_\mu}{\langle dE_\mu/dy \rangle}, \quad (16)$$

where  $E_{\mu, \text{beam}}$  is the initial energy of the incident muon beam. Equation (16) can be used to simplify Eq. (15) into

$$N_S \approx \frac{N_\mu n_{\text{atom}}}{\langle dE_\mu/dy \rangle} \int_{E_{\mu, \min}}^{E_{\mu, \text{beam}}} dE_\mu \int_{x_{\min}}^1 dx \frac{d\sigma_{2 \rightarrow 3}}{dx} (e^{-\frac{z_{\min}}{L_S}} - e^{-\frac{z_{\max}}{L_S}}), \quad (17)$$

where the fiducial range for the decay,  $z_{\min}$  and  $z_{\max}$ , are respectively given by

$$z_{\min}(E_\mu) = L_{\text{tg}} + L_{\text{det}} - \Delta y(E_\mu), \quad z_{\max} = \infty. \quad (18)$$

$L_{\text{tg}}$  and  $L_{\text{det}}$  represent the lengths of the target and detector, respectively. For a lead target,  $n_{\text{atom}} = 3.3 \times 10^{22}/\text{cm}^3$  and  $\langle dE_{\mu}/dy \rangle \approx 12.7 \times 10^{-3} \text{ GeV/cm}$  for the relevant beam energy range [34]. For the thin target ( $L_{\text{tg}} = 0.2 \text{ m}$ ), the muon energy after penetrating the target,  $E_{\mu,\text{min}} = 159.75 \text{ GeV}$ , is close to the incident beam energy  $E_{\mu,\text{beam}} = 160 \text{ GeV}$ .

The signature of the signal at NA64-type experiment for the incoming electron mode is a single EM shower in the target corresponding to the final state electron with significant missing energy. The required missing energy,  $E_{\text{miss}}$ , should be above expected background values. In the muon mode, the detection strategy would be modified somewhat, as one would need to detect the energy of the final state muon. As suggested by [26,29], here we require  $E_{\text{miss}} > E_{\mu,\text{beam}}/3 \approx 53 \text{ GeV}$ , which is equivalent to setting  $x_{\text{min}} = 1/3$  given  $E_{\mu}$  is close to  $E_{\mu,\text{beam}}$  for the thin target of NA64. We further assume the efficiency for the signal reconstruction  $\approx 100\%$  and leave a more detailed detector modeling and study for the future.

## 2. Fermilab muon beam-dump experiment

Fermilab have capabilities of producing a more intense source of muons, albeit at a smaller muon beam energy. We suggest the simplest muon beam dump experiment, where a muon beam is fully stopped in a dense target with a thickness of several meters. Similar to the NA64-type of experiments, we can estimate the number of signal events using existing setup for the Fermilab muon beam. The incident muon beam energy we propose for the experiment,  $E_{\mu,\text{beam}}$ , is  $\sim 3 \text{ GeV}$ , as the accelerator complex is already tuned to this energy for the muon  $g-2$  experiment [35]. Such a beam will be completely stopped in 1.5 m thickness tungsten target ( $n_{\text{atom}} = 6.3 \times 10^{22}/\text{cm}^3$  and  $\langle dE_{\mu}/dy \rangle \approx 22.1 \times 10^{-3} \text{ GeV/cm}$  for the beam energy range [34]). Hence we propose a setup for the Fermilab muon beam-dump experiment as shown in Fig. 1. The lengths of the target (tungsten) and detector are around 1.5 m and 3 m, respectively. The total exposure taken for this proposed experiment is  $10^7$  muons per second for 1 year of running, or  $3 \times 10^{14}$  muons in total on target.

To avoid the background from soft muons, we adopt a lower limit on the muon beam energy  $E_{\mu,\text{min}} = 0.5 \text{ GeV}$ . To estimate the number of signal events, we need to account for the muon energy loss inside the target via an integration over  $E_{\mu}$  from 0.5 GeV to 3 GeV. Here the IWW approximation is not applicable since the muon energy around  $E_{\mu,\text{min}}$  is not much greater than  $m_{\mu}$ . Instead we use MADGRAPH 5 AMC@NLO [36] to obtain the cross sections of  $\sigma(\mu^+ + N \rightarrow \mu^+ + N + S)$  for various  $E_{\mu}$ . The combined atomic and nuclear form factor,  $G_2(t)$ , is implemented in the model file (see Appendix for more details) and the decay probability is implemented by reweighting the generated events. The

procedure yields numerical values of the reweighed cross section

$$\tilde{\sigma}(E_{\mu}) = \int_{x_{\text{min}}}^1 dx \frac{d\sigma_{2 \rightarrow 3}}{dx} \left( e^{-\frac{z_{\text{min}}}{L_S}} - e^{-\frac{z_{\text{max}}}{L_S}} \right) \quad (19)$$

as a function of  $E_{\mu}$ . The fiducial range of the decay here is given by

$$z_{\text{min}}(E_{\mu}) = L_{\text{tg}} - \Delta y(E_{\mu}), \quad z_{\text{max}}(E_{\mu}) = L_{\text{det}} + z_{\text{min}}. \quad (20)$$

To estimate the number of signal events, we interpolate over the samplings of  $\tilde{\sigma}(E_{\mu})$  and perform the integration over  $E_{\mu}$  according to Eq. (17).

The signature of the signal at Fermilab experiment is a decay with a sizable displaced vertex reconstructed from  $e^+e^-$  or  $\gamma\gamma$ . A typical electron or photon tracker/calorimeter requires a minimum momentum/energy of the particle around 10 MeV. This threshold is much smaller than the momentum of the decayed electrons or photons in the lab-frame,  $p_{e,\gamma}^{\text{lab}} \approx \gamma_S m_S/2 = xE_{\mu}/2$ , and hence can be easily satisfied given a small  $x$ . Therefore we approximate  $x_{\text{min}} \approx 0$  in the estimation of  $N_S$ . Like the NA64 case, we further assume the efficiency for the signal reconstruction  $\approx 100\%$  and leave a more careful detector modeling for future experimental studies.

## 3. Difference between setups of NA64-type and Fermilab muon beam-dump experiments

Table I summarizes the setups of NA64-type and Fermilab muon beam-dump experiments. To illustrate the kinematic difference between the two setups, in Fig. 4 we show the decay probabilities of  $S$  within the geometrical acceptance with  $m_S = 100 \text{ MeV}$  in model A (black) and model B (red dashed) for the NA64 (left) and Fermilab (right), respectively. For the NA64-type experiment (Fig. 4, right panel), the curve corresponding to model B (red dashed) rises earlier as we gradually turn off the coupling. This is due to the fact that the decay length of  $S$  in model B is much longer compared to that in model A. Since the fiducial volume is from  $\sim 5 \text{ m}$  to infinity, we find that the decay probabilities remain close to one for very small  $g_{\mu}$ , corresponding to the region of parameter space where the scalars are very long-lived. This tells us that the lower contours of NA64 in Fig. 5 is set by the production rate. Since the production rate of the light scalar is identical in both models A and B as illustrated in Fig. 2, the lower limits for both models for NA 64 in Fig. 4 are the same. For the muon beam-dump experiment at Fermilab, the width of the peak is due the finite size of the detector. Similar to the NA64 case, the curve corresponding to model B (red dashed) peaks earlier as the decrease of the coupling  $g_{\mu}$ .

TABLE I. Parameters for the proposed muon beam-dump experiments at NA64 and Fermilab.

	NA64-type	Fermilab
Incident muon beam energy, $E_{\mu,\text{beam}}$	160 GeV	3 GeV
Total number of incident muons, $N_{\mu}$	$8 \times 10^{12}$	$3 \times 10^{14}$
Target material	Tungsten (W)	Lead (Pb)
Atomic number density, $n_{\text{atom}}$	$3.3 \times 10^{22}/\text{cm}^3$	$6.3 \times 10^{22}/\text{cm}^3$
Muon energy loss per unit length, $\langle dE_{\mu}/dy \rangle$	$12.7 \times 10^{-3} \text{ GeV}/\text{cm}$	$22.1 \times 10^{-3} \text{ GeV}/\text{cm}$
Target Length, $L_{\text{tg}}$	0.2 m	1.5 m
Detector Length, $L_{\text{dec}}$	5 m	4.5 m
Min fiducial range for the decay, $z_{\text{min}}$	$L_{\text{tg}} + L_{\text{dec}} - \Delta y(E_{\mu})$	$L_{\text{tg}} - \Delta y(E_{\mu})$
Max fiducial range for the decay, $z_{\text{max}}$	$\infty$	$L_{\text{tg}} + L_{\text{dec}} - \Delta y(E_{\mu})$

## B. Potential backgrounds

The NA64 experiment has addressed the issues of potential background for the missing energy/momentum search, and many components of the experiment are tuned to reject various sources of backgrounds [26,29]. As described above, those studies suggest a missing energy cut  $E_{\text{miss}} \gtrsim 50 \text{ GeV}$ , which is equivalent to requiring  $1/3 < x < 1$ . A more detailed analysis on potential backgrounds requires knowledge of the detector and is beyond the scope of this paper.

Next, we focus on possible backgrounds to the proposed Fermilab muon beam-dump experiment. All charged particles can be efficiently stopped inside the target given the target length we adopted. Potential backgrounds may arise from the neutral long-lived kaons. They are produced by muons and decay after reaching the detector. They can mimic the long-lived scalars  $S$ . For model B,  $K_L \rightarrow \pi^+ \pi^- \pi^0$  and  $K_L \rightarrow 3\pi^0$  decays are particularly worrisome, as they produce photonlike energy deposition. It is instructive to estimate how many  $K_L$  reach the end of the target without suffering the degradation in energy. To do that we consider the muon-initiated kaon production cross section  $\sigma(\mu + N \rightarrow \mu + K^0 + X)$ , where  $X$  is a baryonic state with

an open strangeness. The cross section size can be estimated using the WW approximation, and related to the underlying kaon photoproduction cross section,

$$d\sigma(\mu + N \rightarrow \mu + K^0 + X) \sim \sigma(N + \gamma \rightarrow K^0 + X) dn_{\gamma}, \quad (21)$$

where  $n_{\gamma}$  is the number of quasireal (or equivalent) photons carried by the muon. The total number of  $K_L$  is then given by

$$N_{\text{kaon}} \simeq \frac{N_{\mu}}{2} \int_{E_{\mu,\text{min}}}^{E_{\mu,\text{beam}}} dE_{\mu} \frac{n_{\text{atom}}}{\langle dE_{\mu}/dy \rangle} \int_{\omega_{\text{min}}}^{\omega_{\text{max}}} \sigma(\omega) dn_{\gamma}(\omega) e^{-\frac{z_{\text{min}}}{L_N}}, \quad (22)$$

where  $\sigma(\omega)$  is the kaon photoproduction cross section with an incident photon energy  $\omega$  on a tungsten nucleus. We assume that the cross section is given by an incoherent sum of the production cross section on individual nucleons,  $\propto A\sigma_{\text{kaon}}$  with  $A$  being the number of nucleons. In turn,  $\sigma_{\text{kaon}}$  receives contributions from several subprocesses,  $\sigma(\gamma + n \rightarrow K^0 + \Lambda)$ ,  $\sigma(\gamma + p \rightarrow K^0 + \Sigma^+)$ , and  $\sigma(\gamma + n \rightarrow K^0 + \Sigma^0)$ . Each of these individual cross

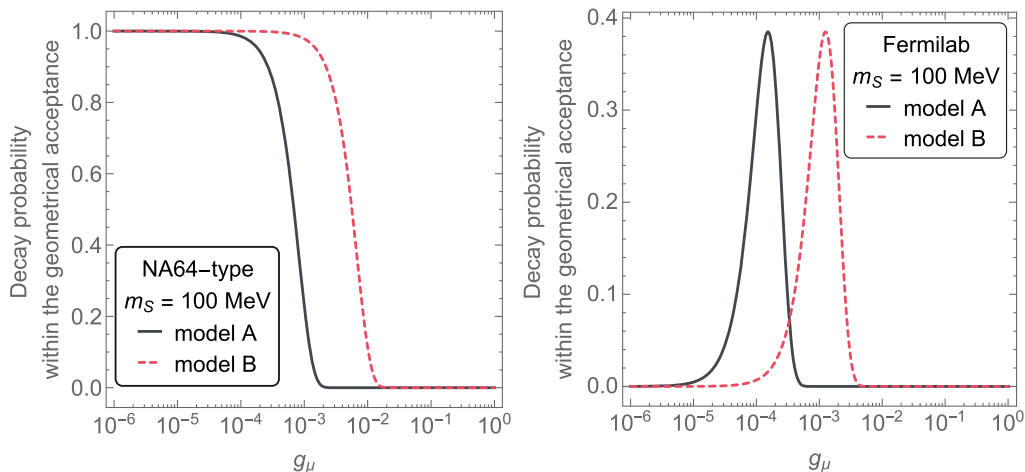


FIG. 4. Decay probabilities of  $S$  within the geometrical acceptance with  $m_S = 100 \text{ MeV}$  in model A (black) and model B (red dashed) at NA64 (left) and Fermilab (right), respectively.

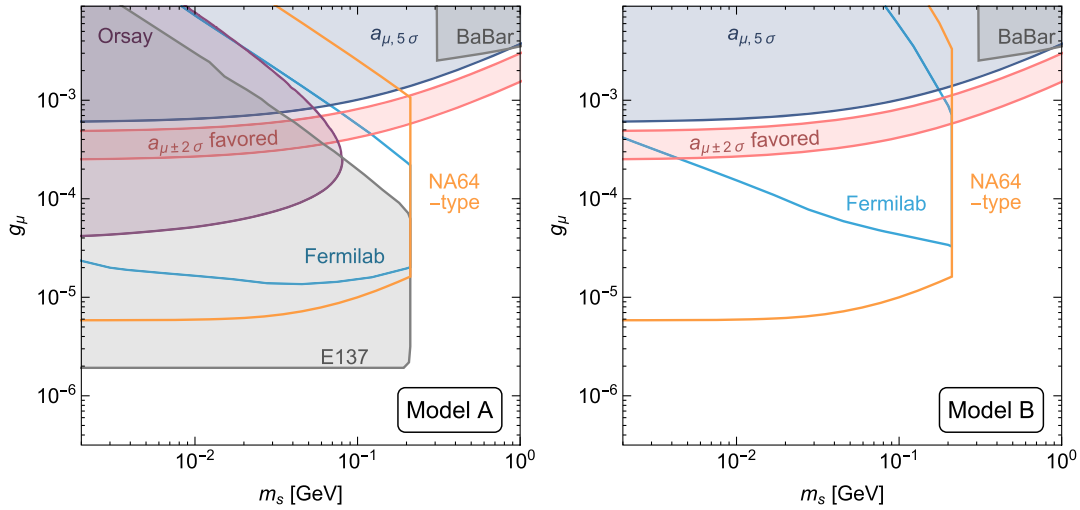


FIG. 5. Prospects and constraints in the  $m_S$  vs.  $g_\mu$  plane for model A (left) and model B (right), respectively. The orange and cyan contours show the projected constraints from NA64-type and Fermilab muon beam-dump experiments, respectively. We include the  $2\sigma$  CL favored region and the  $5\sigma$  CL exclusions of  $a_\mu$  [9,10], and *BABAR* constraints [37] for both models. For model A (left), we also include constraints from Orsay [38] and E137 [39]. See text for more details.

sections is about  $0.8 \mu\text{b}$  on average, and becomes very small for  $\omega < 1.5 \text{ GeV}$  [40–42]. The neutral kaons are produced predominantly in the upstream part of the target, and then propagate through about a meter of dense material. In the process of doing so their energy is degraded, and an idealized factor  $e^{-\frac{z}{L_N}}$  in Eq. (22) is to account for the probability of the produced kaons reaching the end of the target without interaction with the material.  $L_N$  represents the nuclear collision length, which is  $\approx 6 \text{ cm}$  for tungsten. Estimated that way, for one year of running, the number of kaons produced is around  $\mathcal{O}(1)$  before any cuts. We expect that those background events can be further rejected by applying selection criteria, such as absence of charged pions and/or invariant mass cuts. The kaon background can also be reduced by lowering the energy of the incident muon beam. Therefore we neglect the kaon background for Fermilab muon beam-dump in the projection below. More detailed background estimations can be achieved via specialized simulations for a concrete experimental design.

#### IV. RESULTS

Based on the estimations of the number of signal events for the muon beam-dump experiments at NA64 and Fermilab, we project sensitivities for the two proposed experiments for various models. Figure 5 shows the resulting exclusions with 95% confidence level (CL) on the  $m_S$  vs.  $g_\mu$  plane for model A where  $S$  dominantly decays through  $e^+e^-$  (left) and model B where  $S$  decays into  $\gamma\gamma$  via a  $\tau$ -loop (right). The orange and cyan contours on the plots represent constraints from NA64 and Fermilab respectively. The projected constraints from the muon beam-dump

experiments are compared with current constraints and the favored parameter space from other experiments. The red band is the favored region to solve the  $a_\mu$  discrepancy with  $2\sigma$  CL. The blue region are contributions of  $S$  to  $a_\mu$  that excluded with  $5\sigma$  CL. We have also show the limits from electron beam-dump experiments, Orsay [38] (purple) and E137 [39] (gray) for model A. Those limits are not relevant for model B since there  $S$  does not couple to electrons. The *BABAR* collaboration search through the process  $e^+e^- \rightarrow \mu^+\mu^-S$  [37] and excludes the upper right corner of the parameter space for both models.

For model A, the projected constraints from NA64 and Fermilab is largely covered by existing E137 constraint for small  $m_S$  and  $g_\mu$ . Nevertheless, the muon beam-dump experiments will cover new grounds for the range of  $m_S$  from 50 MeV to 210 MeV and  $g_\mu$  from several of  $10^{-5}$  to  $10^{-3}$ . They can effectively exclude the  $a_\mu$  favored region for the  $m_S$  range, which is not reached by E137. The importance of this region of parameter space has also been pointed out by [43] in the context of a more general model, where the authors attempt to address both the muon  $g-2$  anomaly and the proton charge radius puzzle. As for model B, both muon beam-dump experiments at Fermilab and NA64 can place strong limits and completely exclude the parameter space favored by muon  $g-2$  experiment below the di-muon threshold. Again the NA64-type experiment is more sensitive to smaller  $g_\mu$  region comparing to the Fermilab experiment.

#### V. CONCLUSIONS AND DISCUSSIONS

Muon beams have many applications in particle physics. Among fundamental physics applications, they have been

used to study nuclear structure and perform precision measurements of  $g-2$ . The latter presents an intriguing  $3\sigma-4\sigma$  deficit of theoretical predictions relative to experimental observations. It could be a sign of low-mass new physics coupled to muons. All attempts to find such particles so far have rendered only exclusions on masses and couplings of such particles. The majority of those searches have concentrated on hadron or electron-initiated production. In light of the main discrepancy coming from the muon sector, it makes sense to explore the possibility of light particles coupled predominantly to muons, and try to use a muon beam as a source of such particles.

We have shown that muon beam-dump experiments at NA64 and Fermilab can effectively explore the light scalars that are predominantly coupled to muons. Full UV-complete models with such scalars can be built. In this paper we have explored a simplified low-energy version of such models without going into details of the UV completion. The scalar  $S$  can have a small, or vanishing, coupling to electrons. This also make the exotic scalar,  $S$ , long-lived, leading to the displaced decays in the beam-dump experiments. We have found that the experiments with muon beams indeed extend the reach to the parameter space of the exotic scalars. In particular, the favored parameter space to explain the  $a_\mu$  discrepancy can be effectively probed.

Below we would like to discuss additional aspects of the low-mass new physics experiments with muon beams and the models they can explore:

(i) *Practical aspects of muon beam-dump at Fermilab.*

The beam-dump experiment with the anomalous energy deposition downstream from the dump is among the simplest particle physics experiments. The muon beam energies available at Fermilab allow to make this setup relatively compact, with the total length of a few meters. As such this proposed experiment could go into the  $g-2$  experimental hall. Moreover, depending on the availability of protons, the proposed beam-dump can be run in parallel with the  $g-2$  experiment.

- (ii) *Model dependence.* The simplified model of one scalar particle considered in this paper is an example of a physics goal that muon beam-dump experiments may pursue. An interesting variation of this is when the multiplicity of exotic states  $N_d$  is large, as may occur in the models with extra dimensions where the dark forces are allowed to live [44–46], or in models with some conformal dynamics, where the new states are continuously spread over the invariant mass [47]. It is easy to see the qualitative difference in the phenomenology of such models compared to an exotic single state models. The effects of virtual dark force particles (such as corrections to  $g-2$ ) can be enhanced by large multiplicity. Therefore, smaller individual couplings can be responsible for the same size of the corrections. Moreover, the mass step,

$\Delta m_S$ , can lead to overlapping resonances within a detector mass resolution, undermining the “bump hunt” searches. This type of models with, e.g. a tower of dark photons, will escape current direct searches at NA48/2, BABAR etc., but can be a source of sizeable corrections in  $g-2$ . It is easy to see that such models generically lead to longer lifetimes of individual states, and therefore can be subjected to tighter displaced decay bounds. Such models can also be probed in the muon beam-dump experiments.

- (iii) *The advantage of running NA64 in the muon mode.* NA64 experiment currently occupies a unique niche (which can be followed up by a similar experiment in North America [48]). In this paper we have argued that a muon run in NA64 is warranted, as it provides a very strong sensitivity to models (model B) where the decay of  $S$  happens well outside the detector. This adds to an important case of  $L_\mu - L_\tau$  gauge boson with mass  $m_{Z'} < 2m_\mu$ , where the final state of decay is always neutrinos [26].
- (iv) *Neutrino sources, SHiP.* In this paper, we have concentrated on considering dedicated experiments with muon beams. Two other possibilities involve proton beam-dumps, which also creates a lot of muons, as well as beams of mesons used to source the neutrino beams. None of these possibilities is suitable for the missing energy or missing momentum studies. However, the anomalous energy deposition at the distance can indeed be probed, as is well known. Perhaps a very powerful probe of new physics coupled to muons can be achieved at a proposed SHiP facility [27]. There, a large number of muons created in the target propagates through tens of meters of material before getting stopped or deflected. The decay products of the light particles produced in the collision of muons with nuclei can be detected downstream, and a relatively short distance to detector (compared to past proton beam-dump experiments), as well as large boosts, may significantly increase the reach to unexplored parts of parameter space. Constraints on the muonic forces from the proton beam-dumps deserve a separate dedicated study.
- (v) *Tau-initiated production.* Finally, model A with  $g_\ell \propto m_\ell$  can be probed at high-luminosity  $e^+e^-$  colliders through the process  $e^+e^- \rightarrow \tau^+\tau^-S \rightarrow \tau^+\tau^-e^+e^-$  [23]. In light of the discussions in this paper, the decay of  $S$  can also be displaced, producing a rather unique signature that is easy to be distinguished from the SM processes. Both Belle and BABAR collaborations could perform corresponding analyses.

## ACKNOWLEDGMENTS

We would like to thank R. Essig, E. Izaguirre, Y.-S. Liu, G. Magill, D. McKeen, R. Plestid, M. Schmaltz, and



N. Toro for helpful discussions. Y.Z. thanks N. Blinov, R. Essig, E. Izaguirre, V. Khachatryan, O. Mattelaer, A. Simonyan, and M. Takashi for setting up and testing the modified MadGraph 5 event generator for fixed-target experiments. The work of C.-Y.C and M. P. is supported by NSERC, Canada. Research at the Perimeter Institute is supported in part by the Government of Canada through NSERC and by the Province of Ontario through MEDT. Y.Z. is supported through DoE Grant No. DE-SC0015845.

## APPENDIX: ATOMIC AND NUCLEAR FORM FACTORS

The combined atomic and nuclear form factor,  $G_2$ , is presented in [30,31,49,50]. Two components contribute to  $G_2$ : (1) the elastic part is given by

$$G_2^{\text{el}}(t) = \left( \frac{a^2 t}{1 + a^2 t} \right)^2 Z^2 \left( \frac{1}{1 + t/d} \right)^2, \quad (\text{A1})$$

where the virtuality  $t$  represents the momentum transfer squared.  $a = 111Z^{-1/3}/m_e$  under Thomas-Fermi model and  $d = 0.164 \text{ GeV}^2 A^{-2/3}$  where  $A$  and  $Z$  stand for the mass number and atomic number of the target material, respectively.  $m_e$  is the electron mass [30,49,50]; (2) the inelastic part, in the limit  $t/m_p^2$  is small, is given by

$$G_2^{\text{in}}(t) = \left( \frac{a'^2 t}{1 + a'^2 t} \right)^2 Z \left( \frac{1 + t(\mu_p^2 - 1)/(4m_p^2)}{(1 + t/(0.71 \text{ GeV}^2))^4} \right)^2, \quad (\text{A2})$$

where  $m_p$  is the proton mass,  $a' = 773Z^{-2/3}/m_e$ , and  $\mu_p = 2.79$  [30].

For the parameter space of  $m_S$  we are interested in, the expression for  $G_2^{\text{in}}$  is valid, and we do not have to include the inelasticity at the nucleon level. The form factors dress the nucleus-nucleus-photon vertex with  $G_2^{1/2} = (G_2^{\text{el}} + G_2^{\text{in}})^{1/2}$ , which we implement in MADGRAPH 5 AMC@NLO according to [51].

- 
- [1] J. L. Hewett *et al.*, [arXiv:1205.2671](#).
- [2] R. Essig *et al.*, in *Proceedings, Community Summer Study 2013: Snowmass on the Mississippi (CSS2013): Minneapolis, MN, USA* (2013) [[arXiv:1311.0029](#)].
- [3] J. Alexander *et al.*, [arXiv:1608.08632](#).
- [4] J. Jaeckel and A. Ringwald, *Annu. Rev. Nucl. Part. Sci.* **60**, 405 (2010).
- [5] C. Boehm and P. Fayet, *Nucl. Phys.* **B683**, 219 (2004).
- [6] M. Pospelov, A. Ritz, and M. B. Voloshin, *Phys. Lett. B* **662**, 53 (2008).
- [7] N. Arkani-Hamed, D. P. Finkbeiner, T. R. Slatyer, and N. Weiner, *Phys. Rev. D* **79**, 015014 (2009).
- [8] G. W. Bennett *et al.* (Muon g-2), *Phys. Rev. D* **73**, 072003 (2006).
- [9] J. Grange *et al.* (Muon g-2), [arXiv:1501.06858](#).
- [10] T. Mibe (J-PARC g-2), *Chin. Phys. C* **34**, 745 (2010).
- [11] M. Benayoun *et al.* [[arXiv:1407.4021](#)].
- [12] L. Jin, T. Blum, N. Christ, M. Hayakawa, T. Izubuchi, C. Jung, and C. Lehner, in *Proceedings, 34th International Symposium on Lattice Field Theory (Lattice 2016): Southampton, UK* (2016) [[arXiv:1611.08685](#)].
- [13] R. Pohl *et al.*, *Nature (London)* **466**, 213 (2010).
- [14] A. Antognini *et al.*, *Science* **339**, 417 (2013).
- [15] R. Pohl *et al.* (CREMA Collaboration), *Science* **353**, 669 (2016).
- [16] P. J. Mohr, D. B. Newell, and B. N. Taylor, *Rev. Mod. Phys.* **88**, 035009 (2016).
- [17] S. N. Gninenko and N. V. Krasnikov, *Phys. Lett. B* **513**, 119 (2001).
- [18] P. Fayet, *Phys. Rev. D* **75**, 115017 (2007).
- [19] M. Pospelov, *Phys. Rev. D* **80**, 095002 (2009).
- [20] W. Altmannshofer, S. Gori, M. Pospelov, and I. Yavin, *Phys. Rev. Lett.* **113**, 091801 (2014).
- [21] W. Altmannshofer, C.-Y. Chen, P. S. B. Dev, and A. Soni, *Phys. Lett. B* **762**, 389 (2016).
- [22] C.-Y. Chen, H. Davoudiasl, W. J. Marciano, and C. Zhang, *Phys. Rev. D* **93**, 035006 (2016).
- [23] B. Batell, N. Lange, D. McKeen, M. Pospelov, and A. Ritz, *Phys. Rev. D* **95**, 075003 (2017).
- [24] R. Aaij *et al.* (LHCb Collaboration), *Phys. Rev. Lett.* **115**, 161802 (2015).
- [25] S. Andreas *et al.*, *Phys. Rev. D* **89**, 075008 (2014).
- [26] S. N. Gninenko, N. V. Krasnikov, and V. A. Matveev, *Phys. Rev. D* **91**, 095015 (2015).
- [27] S. Alekhin *et al.*, *Rept. Prog. Phys.* **79**, 124201 (2016).
- [28] R. Essig, R. Harnik, J. Kaplan, and N. Toro, *Phys. Rev. D* **82**, 113008 (2010).
- [29] D. Banerjee *et al.* (NA64 Collaboration), *Phys. Rev. Lett.* **118**, 011802 (2017).
- [30] K. J. Kim and Y.-S. Tsai, *Phys. Rev. D* **8**, 3109 (1973).
- [31] J. D. Bjorken, R. Essig, P. Schuster, and N. Toro, *Phys. Rev. D* **80**, 075018 (2009).
- [32] Y.-S. Liu, D. McKeen, and G. A. Miller, *Phys. Rev. D* **95**, 036010 (2017).
- [33] C. Patrignani *et al.* (Particle Data Group Collaboration), *Chin. Phys. C* **40**, 100001 (2016).
- [34] <http://pdg.lbl.gov/2015/AtomicNuclearProperties/>.
- [35] A. Chapelain, *EPJ Web Conf.* **137**, 08001 (2017).
- [36] J. Alwall, R. Frederix, S. Frixione, V. Hirschi, F. Maltoni, O. Mattelaer, H. S. Shao, T. Stelzer, P. Torrielli, and M. Zaro, *J. High Energy Phys.* **07** (2014) 079.

- [37] J. P. Lees *et al.* (BABAR Collaboration), *Phys. Rev. D* **94**, 011102 (2016).
- [38] M. Davier and H. Nguyen Ngoc, *Phys. Lett. B* **229**, 150 (1989).
- [39] J. D. Bjorken, S. Ecklund, W. R. Nelson, A. Abashian, C. Church, B. Lu, L. W. Mo, T. A. Nunamaker, and P. Rassmann, *Phys. Rev. D* **38**, 3375 (1988).
- [40] S. Goers *et al.* (SAPHIR), *Phys. Lett. B* **464**, 331 (1999).
- [41] K. Tsukada *et al.*, *Phys. Rev. C* **78**, 014001 (2008); **83**, 039904(E) (2011).
- [42] Maeda and Kazushige, <http://www.rcnp.osaka-u.ac.jp/~baryons/08/Metting%20Room3/maeda.pdf>.
- [43] Y.-S. Liu, D. McKeen, and G. A. Miller, *Phys. Rev. Lett.* **117**, 101801 (2016).
- [44] K. L. McDonald and D. E. Morrissey, *J. High Energy Phys.* **05** (2010) 056.
- [45] C. J. Wallace, J. Jaeckel, and S. Roy, in *Proceedings, 9th Patras Workshop on Axions, WIMPs and WISPs (AXION-WIMP 2013): Mainz, Germany* (2013) [arXiv:1311.6415].
- [46] J. Jaeckel, S. Roy, and C. J. Wallace, arXiv:1408.0019.
- [47] H. Georgi, *Phys. Rev. Lett.* **98**, 221601 (2007).
- [48] E. Izaguirre, G. Krnjaic, P. Schuster, and N. Toro, *Phys. Rev. D* **91**, 094026 (2015).
- [49] Y.-S. Tsai, *Rev. Mod. Phys.* **46**, 815 (1974); **49**, 421 (1977).
- [50] Y.-S. Tsai, *Phys. Rev. D* **34**, 1326 (1986).
- [51] <https://cp3.irmp.ucl.ac.be/projects/madgraph/wiki/FormFactors>.